Efficient Perovskite Solar Cells over a Broad Temperature Window

Shao, Shuyan; Liu, Jian; Fang, Hong-Hua; Qiu, Li; ten Brink, Gert H.; Hummelen, Jan C.; Koster, L. Jan Anton; Loi, Maria Antonietta

Published in:
Advanced Energy Materials

DOI:
10.1002/aenm.201701305

Publication date:
2017

Efficient Perovskite Solar Cells over a Broad Temperature Window: The Role of the Charge Carrier Extraction

*Shuyan Shao, Jian Liu, Hong-Hua Fang, Li Qiu, Gert H. ten Brink, Jan C. Hummelen, L. Jan Anton Koster, and Maria Antonietta Loi**

The mechanism behind the temperature dependence of the device performance in hybrid perovskite solar cells (HPSCs) is investigated systematically. The power conversion efficiency (PCE) of the reference cell using [60]PCBM as electron extraction layer (EEL) drops significantly from 11.9% at 295 K to 7% at 180 K. The deteriorated charge carrier extraction is found as the dominant factor causing this degradation. Temperature dependent spectroscopy and charge transport studies demonstrate that the poor electron transport in the [60]PCBM EEL at low temperature leads to inefficient charge carrier extraction. It is further demonstrated that the n-type doping of [60]PCBM EEL or the use of an EEL (fulleropyrrolidine with a triethylene glycol monoethyl ether side chain) with higher electron transport capability is an effective strategy to achieve HPSCs working efficiently over a broad temperature range. The devices fabricated with these highly performing EELs have PCEs at 180 K of 16.7% and 18.2%, respectively. These results support the idea that the temperature dependence of the electron transport in the EELs limits the device performance in HPSCs, especially at lower temperatures and they also give directions toward further improvement of the PCE of HPSCs at realistic operating temperatures.

1. Introduction

The hybrid perovskite solar cells (HPSCs) have undergone an unprecedented fast increase in power conversion efficiency (PCE) from around 3.8% in 2009 to about 22% in 2017.[1] In the past years, most efforts have been devoted to improve the PCE of this kind of solar cells by developing various device structures, interfacial layers, and strategies to control perovskite film growth.[2–8] Despite the great progress in device performance, there are still several issues to be addressed in order to bring this new technology to a possible commercialization. One of the main concerns is about the performance of this kind of solar cells when temperature varies. Recent studies indicated that the device performance decay upon prolonged exposure to elevated temperatures (>80 °C) due to the chemical decomposition of the perovskite film.[9,10] Several independent research groups have shown progress to improve the thermal stability of HPSCs by developing more stable hybrid perovskites.[10–12] However, the effect of lower temperatures on device performance has been mostly overlooked.

Recently, it was reported that the performance of HPSCs also decays significantly at low temperatures.[13,14] Cojocaru et al. proposed that the deterioration of the device performance at low temperature is caused by the slow diffusion of the charge carriers in the device.[14] Zhang et al. proposed that the deteriorated short circuit current density (J_{SC}) and fill factor (FF) at low temperatures could be caused by the ferroelectric properties of the orthorhombic phase or the incomplete dissociation of the Wannier excitons in the bulk of the perovskite or at the interfaces with electron and hole selective contacts.[15] However, these are still unverified suppositions. So far, temperature dependent studies on HPSCs have been very limited compared to the numerous studies on improving their power output at room temperature. Temperature dependent measurements of HPSCs could be very important to fully understand their operation, and therefore provide a direction to develop effective strategies to further improve their performance.

Herein, we investigate the mechanism for the temperature dependence of the device performance in p–i–n planar perovskite solar cells. We demonstrate that the temperature dependence of the charge extraction is the main underlying

Dr. S. Shao, Dr. J. Liu, Dr. H.-H. Fang, Dr. L. J. A. Koster, Prof. M. A. Loi
Photophysics and OptoElectronics
Zernike Institute for Advanced Materials
University of Groningen
Nijenborgh 4, 9747 AG, Groningen, The Netherlands
E-mail: m.a.loi@rug.nl
Dr. L. Qiu, Prof. J. C. Hummelen
Chemistry of (Bio)organic Materials and Devices
Stratingh Institute for Chemistry
University of Groningen
Nijenborgh 4, 9747 AG, Groningen, The Netherlands
Dr. L. Qiu, Prof. J. C. Hummelen
Zernike Institute for Advanced Materials
University of Groningen
Nijenborgh 4, 9747 AG, Groningen, The Netherlands
G. H. ten Brink
Nanostructured Materials and Interfaces
Zernike Institute for Advanced Materials
University of Groningen
Nijenborgh 4, 9747 AG, Groningen, The Netherlands

DOI: 10.1002/aenm.201701305

reason for the temperature dependence of the performance of HPSCs and that the electron transport capability of electron extraction layers (EELs) dominates the charge extraction in the devices. More specifically, the devices using [60]PCBM EEL show degradation of performance with decreasing temperature due to the degraded charge extraction caused by the poor electron transport in [60]PCBM EEL at low temperature. We show, for the first time, that n-doping of the [60]PCBM EEL or the use of an EEL with higher conductivity is an effective strategy to improve the charge extraction and therefore achieve HPSCs working efficiently over a broad temperature range.

When the more conductive fulleropyrrolidine with a triethylene glycol monoethyl ether side chain (PTEG-1)[16] is used as EEL, the charge extraction is surprisingly efficient over a broad temperature range. The J_{SC} (≈21.2 mA cm^{-2}) and FF (≈0.8) stay relatively constant down to 140 K. Moreover, this is accompanied by an increase in open circuit voltage V_{OC} (from 0.93 to 1.08 V), which result in an overall increase of the PCE from 16.03% (295 K) to 18.16% (180 K), followed by a slight decrease to 17.61% at 140 K. Furthermore, the electron transport of the [60]PCBM layer is improved by n-doping with poly [(9,9-bis(3′-(*N*,*N*-dimethylamino)propyl)-2,7-fluorene)-alt-2,7-(9,9-dioctylfluorene)] (PFN) and LiF (upon thermal treatment). Devices fabricated in this way show similar low temperature performance as devices with PTEG-1 EEL, verifying that the transport properties of the EEL are a main limiting factor for the HPSCs device performance.

2. Results and Discussion

Hybrid perovskite solar cells using a p–i–n device structure were fabricated as shown in our previous work.[7] **Figure 1**a shows the structure where Indium Tin Oxide (ITO) functions as anode, Poly(3,4-ethylenedioxythiophene):Poly(styrenesulfonate) (PEDOT:PSS) as hole transport layer, the mixed halide perovskite $CH_3NH_3PbI_{3-x}Cl_x$ as photon absorbing layer, fullerene derivatives of different types as EEL, and Al as the cathode.

We first investigate how the perovskite film morphology affects the temperature dependence of the *J*–*V* characteristics in HPSCs using [60]PCBM as EEL. We prepared perovskite films with compact and noncompact morphology following procedures reported in one of our previous works (Figure S1, Supporting Information).[17] Recently, we showed that a noncompact perovskite film is the cause of a strong light soaking effect in HPSCs due to severe trap assisted recombination at the grain boundaries.[17] Figure 1b shows how the *J*–*V* curve of an HPSC using a noncompact perovskite film varies as a function of temperature. The measurements are not showing the light soaking effect, i.e., they are performed just after illumination of the device. The photovoltaic parameters of the presented devices are listed in Table S1 and Figure S2 (Supporting Information). At 295 K and under 100 mW cm^{-2} AM 1.5 simulated illumination, the device has a V_{OC} of 0.41 V, a J_{SC} of 20.73 mA cm^{-2}, an FF of 0.48, and PCE of 4.12%. When the temperature is decreased, the FF decreases monotonically

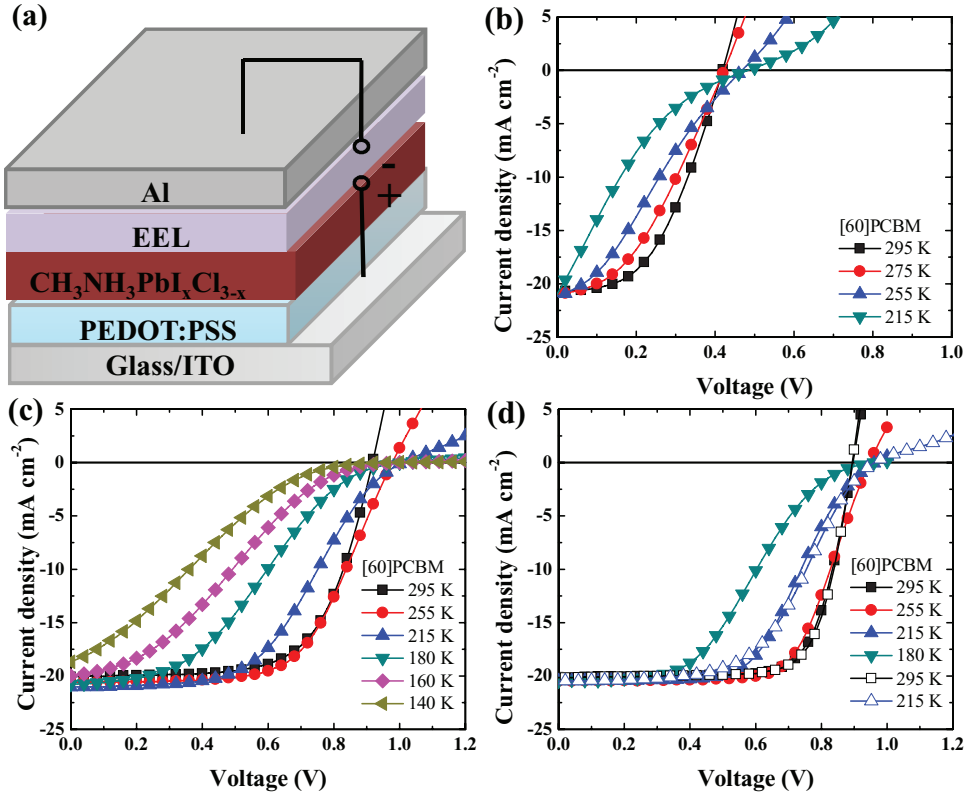

Figure 1. a) Schematic of the device structure used in this work. Temperature dependence of the *J*–*V* curves under illumination of the HPSC using a noncompact perovskite film, b) before light soaking and c) after light soaking. d) Temperature dependence of the *J*–*V* curves under illumination of the HPSC using a compact perovskite film after light soaking.

to 0.14 at 215 K and a prominent S-shape kink appears in the *J–V* curves, which becomes more pronounced with further decreasing of the temperature. These variations of shape indicate deterioration of the charge extraction as temperature decreases, overall the PCE decreases down to 1.41% at 140 K.

These experimental results raise the question whether the traps in the perovskite film are the dominating cause of the temperature dependence of the charge extraction. To answer this question, we tested the temperature dependence of the *J–V* curves after fully soaking the device under illumination at 1 sun for 90 min. The results are shown in Figure 1c. The soaked devices show on average a V_{OC} of 0.90 V, a J_{SC} of 20.1 mA cm^{-2}, an FF of 0.66, and a PCE of 11.9%. The improved device performance such as FF and V_{OC} is attributed to the filling of the traps by the photogenerated carriers.[17,18] After light soaking, when we lower the device temperature, we observe a similar temperature dependence of the device performance as the one observed without light soaking (see Figure 1c and Table S1, Supporting Information).

Figure S3 (Supporting Information) shows the *J–V* curves under dark conditions at various temperatures. By fitting the dark *J–V* curves with the Shockley diode equation, we extracted the series resistance (R_S), and reverse saturation current density (J_0). With decreasing temperature, the R_S increases sharply from 9.4 Ω cm^2 at 295 K to over 300 Ω cm^2 at 215 K. This significant increase in the series resistance results in a barrier that strongly deteriorates the charge extraction. The decreased J_0 explains the increased V_{OC} at low temperature.[19]

From the light intensity dependent V_{OC} measurements of the soaked device, we found that the trap-assisted recombination is suppressed with decreasing temperature, which is evidenced by the smaller value of the slope (n) of the line in the plot reported in Figure S4 (Supporting Information).[17] This can be explained by a reduced trap density in the perovskite film at low temperature, which will be discussed in more detail later. Overall, it appears that at low temperature, trap induced recombination is not the main loss mechanism for charge carriers.

We proceeded to measure devices with compact perovskite film, which have much lower trap density and therefore display negligible light soaking.[17] Once again, we observe, as shown in Figure 1d, a deterioration of the charge extraction with decreasing temperature. It is noteworthy that the temperature dependence of the *J–V* curves is fully reversible when temperature cycles are measured. This is an indication that the temperature dependence of the device performance is an intrinsic phenomenon of the active material and/or of the device structure. Considering the variation in device performance from batch to batch, we repeated the measurements for six different batches of HPSCs having two perovskite film morphologies. Our results indicate that the temperature dependence of the device performance is a property of the device structure and is independent on the perovskite film morphology and on the initial device performance.

Figure 2 shows the light intensity dependent photocurrent of the device fabricated with a noncompact perovskite film measured at different applied voltages (V_a) and temperatures. The slope of the photocurrent on a logarithmic scale versus light intensity depends not only on the applied voltage but also on the temperature. At 295 K, the plots have slopes close to 1 at different V_a, indicating efficient charge carrier extraction and negligible bimolecular recombination (Figure 2a). When the temperature is decreased, the plot exhibits a lower slope when V_a is closer to the maximum power point, indicating that significant bimolecular recombination occurs in the device. The bimolecular recombination turns to be more pronounced with increasing V_a and decreasing temperature (Figure 2b,c). This

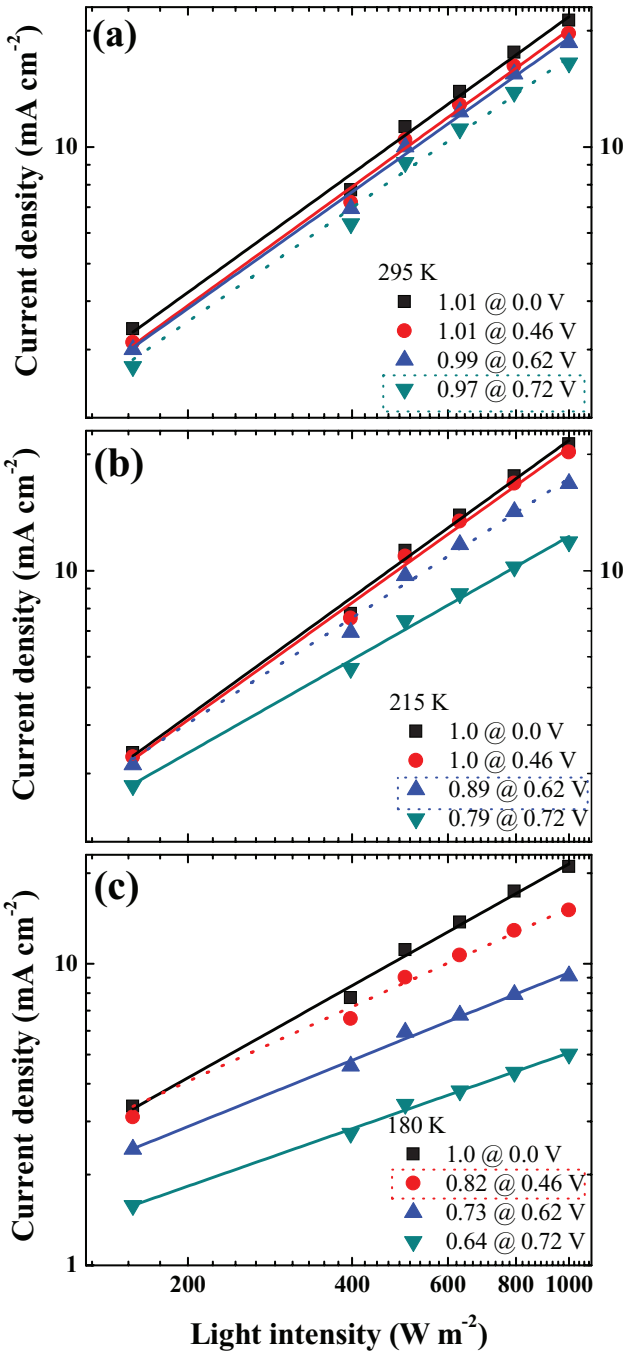

Figure 2. Light intensity dependent photocurrent measured at different applied voltages in the device using [60]PCBM as EEL at a) 295 K, b) 215 K, and c) 180 K. Symbols represent the experimental data, lines represent the fitted results, and the dash lines represent the fitting results with V_a around maximum power point.

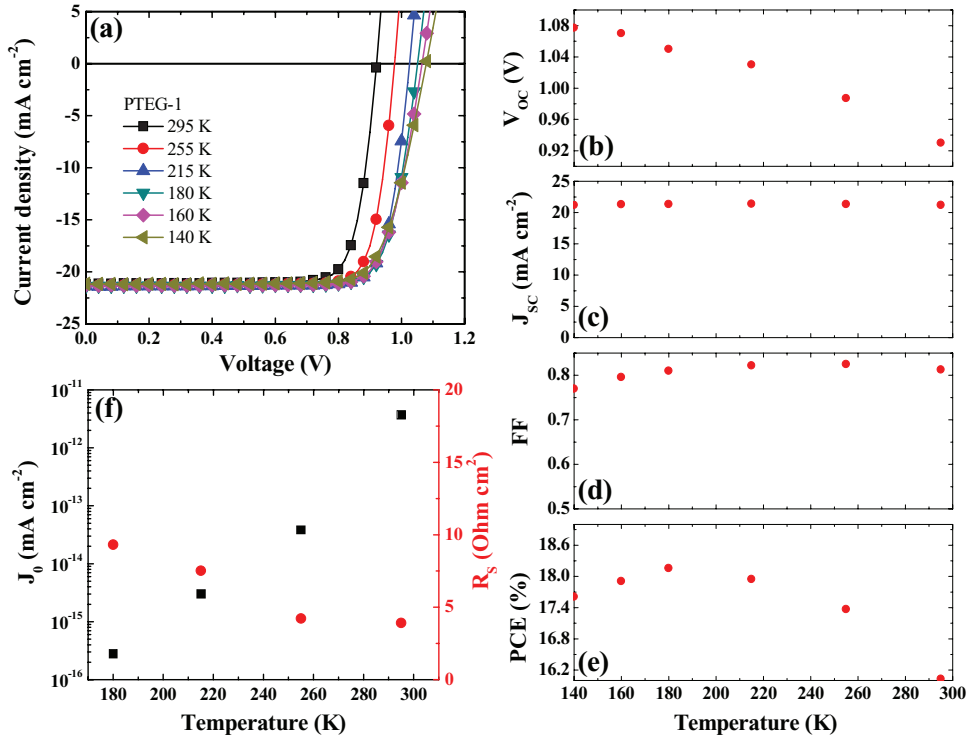

Figure 3. a) Temperature dependence of the *J–V* curves for the HPSC using PTEG-1 as EEL under illumination. Variation of the b) V_{OC}, c) J_{SC}, d) FF, e) PCE, and f) reverse saturation current J_0 and series resistance R_S with temperature.

explains the voltage and temperature dependence of the charge extraction observed in the above HPSCs. Among the possible factors causing this behavior are: (i) a charge injection barrier at the electrode interface, (ii) charge separation barrier at EEL (HEL)/HP interface, and (iii) unbalanced charge transport in the device. For simplicity, compact perovskite films only will be used in the following studies unless otherwise stated.

In our recent work, we have shown that when [60]PCBM is replaced by PTEG-1 as EEL, HPSCs with higher efficiency at room temperature are obtained.[18] In **Figure 3**a we show the temperature dependence of the device performance of HPSCs using PTEG-1 as EEL. We observe two distinct features in the *J–V* curves. The first striking feature is the absence of the S-kink in the *J–V* curves down to 140 K. The second one is the overall positive evolution of the device parameters when lowering the temperature as shown in Figure 3b–e and **Table 1**. The V_{OC} increases from 0.93 to 1.08 V, while J_{SC} stays almost constant around 21 mA cm^{-2}. It is interesting that the FF also stays at high values (≈0.80), decreasing slightly only at 140 K. As a consequence, the PCE of the device increases from 16.03% at 295 K to 18.16% at 180 K, and at 140 K still has a PCE of 17.61%, which is much higher than its room temperature performance.

The weak field and temperature dependence of the photocurrent indicates efficient charge extraction over a broad temperature window, which is explained by the small series resistance (R_S) of the device, showing negligible increase with decreasing temperature (Figure 3f and Figure S5, Supporting Information). Therefore, the bimolecular recombination is negligible and independent on the applied voltage and temperature (Figure S6, Supporting Information).

These results provide evidence that the electron transport layer is dominating the temperature dependence of the device performance. Since the compact perovskite film prevents the penetration of PTEG-1 into the HP layer, we do not expect any

Table 1. Figures of merit of the devices using PTEG-1, [60]PCBM/PFN, and [60]PCBM/TA-PFN as EELs at various temperatures.

Device	Temperature [K]	V_{OC} [V]	J_{SC} [mA cm^{-2}]	FF	PCE [%]
PTEG-1	295	0.93	21.20	0.81	16.03
	255	0.99	21.33	0.83	17.37
	215	1.03	21.41	0.82	17.95
	180	1.05	21.35	0.81	18.16
	160	1.07	21.35	0.80	17.91
	140	1.08	21.20	0.77	17.61
[60]PCBM/PFN	295	0.88	20.20	0.75	13.78
	255	0.92	20.57	0.72	13.76
	235	0.94	20.81	0.59	11.62
	215	0.96	21.20	0.48	9.89
	180	0.96	20.87	0.39	7.90
[60]PCBM/TA-PFN	295	0.91	21.00	0.81	15.48
	255	0.96	21.26	0.83	16.82
	215	0.99	21.35	0.82	17.37
	180	1.00	21.37	0.78	16.67
	160	1.01	21.46	0.73	15.82

significant change in the bulk properties of the perovskite film or the anode/perovskite interfacial properties.

We therefore turn our attention to investigate whether a charge injection barrier at the [60]PCBM/electrode interface affects the temperature dependence of the charge extraction. Previous studies indicate that the $PC_{60}BM$ layer might fail to form an ideal ohmic contact with Al electrodes for efficient charge extraction.[20,21] To solve this issue, a thin layer of PFN or LiF was inserted between the [60]PC_{60}BM/Al interface.[20–22] In our case, the HPSCs using [60]PCBM/PFN or [60]PCBM/LiF EEL layers share some common features in the temperature dependent *J–V* curves with the device using [60]PCBM only as EEL (**Figure 4**a and Figure S7a, Supporting Information). In particular, the photovoltaic parameters, such as V_{OC}, FF, and PCE, show similar variation with decreasing temperature (Figure 4c–f and Table S2, Supporting Information). We note that the pronounced S-shape appears in the *J–V* curves at 180 K. Concurrently, the R_S increases significantly from 3 to 155 Ω cm^2 (Figure S8, Supporting Information). From these experiments we conclude that it is not the EEL/cathode interface to cause the considerable increase in the series resistance and the deterioration of the charge extraction at low temperature.

We therefore fabricated new devices where after deposition of the PFN and LiF thin layer, the whole stack was thermally annealed at 100 °C for 10 min (hereafter referred to as TA-PFN and TA-LiF). These new devices gave rise to very different features in the *J–V* curves compared to the device without thermal annealing, as shown in Figure 4b and Figure S7d (Supporting Information). Similarly to devices using PTEG-1 as EEL, the charge extraction becomes efficient over a broad temperature range and the S-shape kink disappears in the *J–V* curves also for temperatures lower than 160 K. The FF of the devices stays relatively constant from 295 to 180 K (≈0.80), which is followed by a slight decrease with decreasing temperature to 160 K (≈0.73). At the same time, the PCE increases from 15.50% at 295 K to 17.37% at 215 K. At 160 K, the device still has a high PCE of 15.82%. Compared to the counterparts without thermal annealing, the devices using both [60]PCBM/TA-PFN and [60]PCBM/TA-LiF have significantly improved FF and PCE in the tested temperature range. The reason for the dissimilar behavior is that the thermally annealed devices have smaller series resistance and enable efficient charge extraction over the broad temperature range (Figures S7f and S8d, Supporting Information). It is also important to note that Kelvin Probe measurements show that the thermal annealing does not change significantly the energy alignment at the cathode interface.

In order to elucidate the role of the thermal annealing, we thermally annealed devices using only a pristine [60]PCBM layer as EEL. Recent work by Huang and co-workers indicated that thermal annealing of [60]PCBM could passivate traps in the perovskite film.[23] In our case, the thermal treatment of [60]PCBM yields device performance with identical temperature dependence as shown by the devices without thermal annealing (Figure S9, Supporting Information). Once again, these results

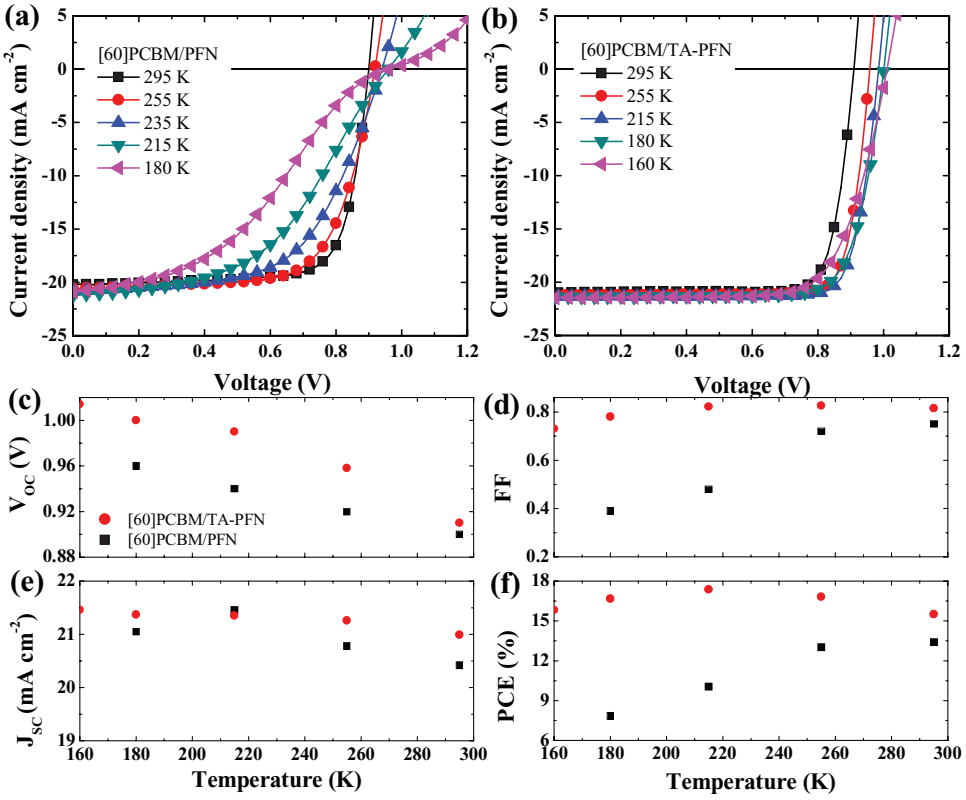

Figure 4. Temperature dependence of the *J–V* curves under illumination for devices using a) [60]PCBM/PFN EEL, b) [60]PCBM/TA-PFN EEL, and the corresponding variation in device parameters c) V_{OC}, d) FF, e) J_{SC}, and f) PCE.

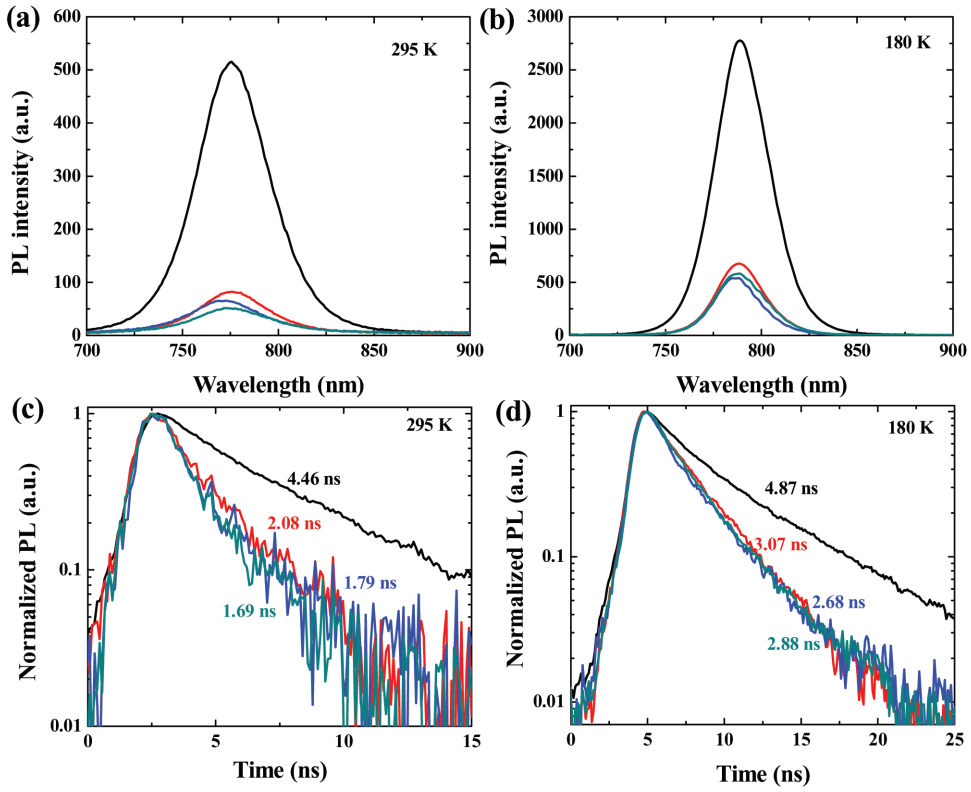

Figure 5. a,b) Steady state and c,d) time resolved PL data recorded at 295 and 180 K, respectively, for the pristine perovskite (black lines), perovskite/PTEG-1 (red lines), perovskite/[60]PCBM (blue lines), and perovskite/[60]PCBM/TA-PFN (dark cyan lines) samples.

prove that traps in perovskite films are not the main reason for the temperature dependent charge extraction behavior. Instead, the thermal annealing seems to change the electrical properties of the [60]PCBM layer or the perovskite/[60]PCBM interface in the presence of PFN or LiF.

To clarify the role of the EELs, we performed temperature dependent steady state and time-resolved photoluminescence (PL) measurements (**Figure 5**). Efficient PL quenching of the perovskite film occurs upon deposition of [60]PCBM, PTEG-1, or [60]PCBM/TA-PFN. Our observation is in agreement with recent studies, showing efficient electrons transfer from perovskites toward fullerene.[24,25] The extent of the PL quenching by all the EELs is similar at high and low temperature, showing that the electron transfer occurs with similar efficiency at different temperatures. At low temperature, the enhanced PL emission of the perovskite layer is an indication of higher band-to-band recombination of the free electrons and holes, lower nonradiative recombination due to the deactivated traps and lower photon scattering (Figure S10, Supporting Information).[26,27] These observations are also verified by time-resolved PL measurements, which show longer emission lifetimes at low temperatures (Figure 5d and Figure S11, Supporting Information).

From the previous discussion, we find that the trap-assisted recombination, band-to-band recombination in perovskite and the contact barriers at the EEL/Al interface are not the main factors to explain the discrepancy in the temperature dependence of the charge extraction in devices using different EELs. The remaining unexplored factor is the charge transport in the EEL. Due to the high conductivity of the PEDOT:PSS HEL and high hole/electron mobility in the perovskite layer, the electron transport in EELs could be the limiting step for the charge extraction. The charge transport occurs via hopping between localized sites in disordered organic semiconductor materials, such as [60]PCBM.[28–30] The distribution of the on-site energy is assumed to be Gaussian due to fluctuation in the local environment. The charge carriers are localized in the density of states (DOS) and they only contribute to the charge transport when they are thermally activated above the transport energy level (E_T) as shown in **Figure 6**a.[29] Therefore, the distance of the E_F to E_T determines the activation energy for the charge transport. Since the thermal energy decreases with decreasing temperature, a lower number of electrons could be activated to the E_T, resulting in their trapping in the tail of the DOS. In the case of high carrier density by n-type doping, the Fermi level (E_F) of [60]PCBM film shifts toward the E_T and therefore reduces the activation energy (see Figure 6b). The electrons therefore can be easily activated to the E_T even though the temperature decreases.

To verify this idea we measured the conductivities of the HP layer and of all EELs at different temperatures as shown in Figure 6c. The pristine [60]PCBM film exhibits a typically low conductivity of 1.6×10^{-9} S cm^{-1} at room temperature, which could not be reliably measured at low temperature because of the low value. The deposition of PFN or LiF on top of [60]PCBM layer did not improve its conductivity significantly.

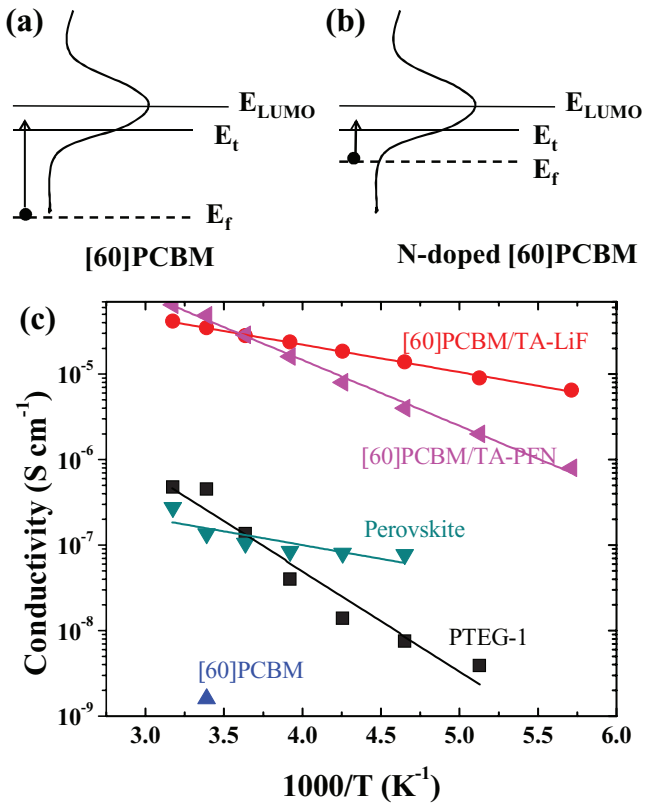

Figure 6. Schematic diagram of the E_F and the E_T in the case of a) pristine [60]PCBM and b) n-doped [60]PCBM, c) the temperature dependence of the conductivity for the perovskite (dark cyan triangle), [60]PCBM (blue triangle), [60]PCBM/TA-LiF (red circle), [60]PCBM/TA-PFN (pink triangle), and PTEG-1 (black square) samples.

However, after thermal annealing, the conductivity of [60]PCBM is improved by four orders of magnitude, indicating that PFN and LiF provide an effective n-doping for [60]PCBM.

It is worth mentioning that for the first time we provide evidences that PFN can n-dope [60]PCBM and we show the first use of PFN or LiF n-doped [60]PCBM EEL in HPSCs. Very recently, Torabi et al. demonstrated that LiF n-dopes [60]PCBM.[31] The pristine PTEG-1 film shows a conductivity of 4×10^{-7} S cm^{-1}, which is over 200 times the one of pristine [60]PCBM. The variation of the conductivity in different EELs with temperature follows the classic Arrhenius equation very well, confirming the thermally activated charge transport. By fitting the temperature dependence of the conductivities, we obtained the activation energy of 0.156 eV for [60]PCBM/TA-PFN, 0.064 eV for [60]PCBM/TA-LiF, and 0.235 eV for PTEG-1, respectively. A previous study reported an activation energy of 0.650 eV for an evaporated C_{60} film.[30] Given the larger molecular disorder of [60]PCBM film than neat C_{60} film, the activation energy of a [60]PCBM film should be even higher.

The temperature dependence of the electron transport properties of the EELs explains the discrepancy in temperature dependence of the charge extraction in HPSCs using different EELs (**Figure 7**). At room temperature, due to the inefficient electron transport in [60]PCBM, a very small band bending occurs at the HP/[60]PCBM interface but it does not cause severe accumulation of holes/electrons at the interface. As the electron transport slows down with the decreasing temperature, the series resistance increases and more photogenerated electrons and holes accumulate at $PC_{60}BM$/HP interface, leading to higher band bending. When the temperature is further lowered down to 180 K, the electrical potential across the [60]PCBM layer limits the transport of electrons. As a consequence, these electrons recombine with the accumulated holes in perovskite film before they reach the respective electrodes, leading to severe interfacial recombination. At the opposite, in the tested temperature range, the conductivity of PTEG-1, [60]PCBM/TA-PFN, and [60]PCBM/TA-LiF is higher than that of [60]PCBM at room temperature due to higher charge carrier density. Therefore, electrons can move toward the cathode efficiently before interfacial recombination occurs. This explains why the HPSCs using PTEG-1 or n-doped [60]PCBM as EEL works efficiently over a very broad temperature range. The devices using PFN or LiF n-doped $PC_{60}BM$ as EEL show a slight decrease of the FF at temperature <180 K. The possible reason is that there is a doping gradient along the charge transport direction, and a very thin and mildly doped [60]PCBM layer is formed adjacently to the perovskite film. As a result, the series resistance arising from this thin layer of [60]PCBM increases so that the charge extraction becomes less efficient at temperature <180 K (see Figure S8d, Supporting Information).

Since the S-shape in the *J–V* curves appear as caused by the pile-up of electrons/holes at the [60]PCBM/HP interface, reducing the photogenerated charges carriers in the HP layer could help to eliminate it. To verify this idea, we measured the light intensity dependence of *J–V* characteristics in devices using different EELs at 215 K, measurements are shown in **Figure 8**. The devices using [60]PCBM as EEL show a less

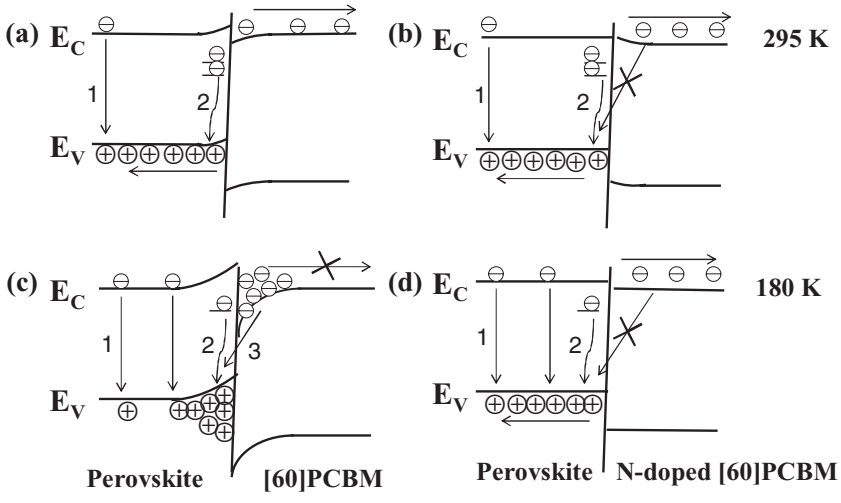

Figure 7. Schematic diagram for the charge extraction and recombination at maximum power point at 295 K (top) and 180 K (bottom) for a,c) the HP/[60]PCBM and b,d) the HP/n-doped [60]PCBM interface. Note: 1 represents band-to-band recombination, 2 represents the trap-assisted recombination, and 3 represents interfacial recombination.

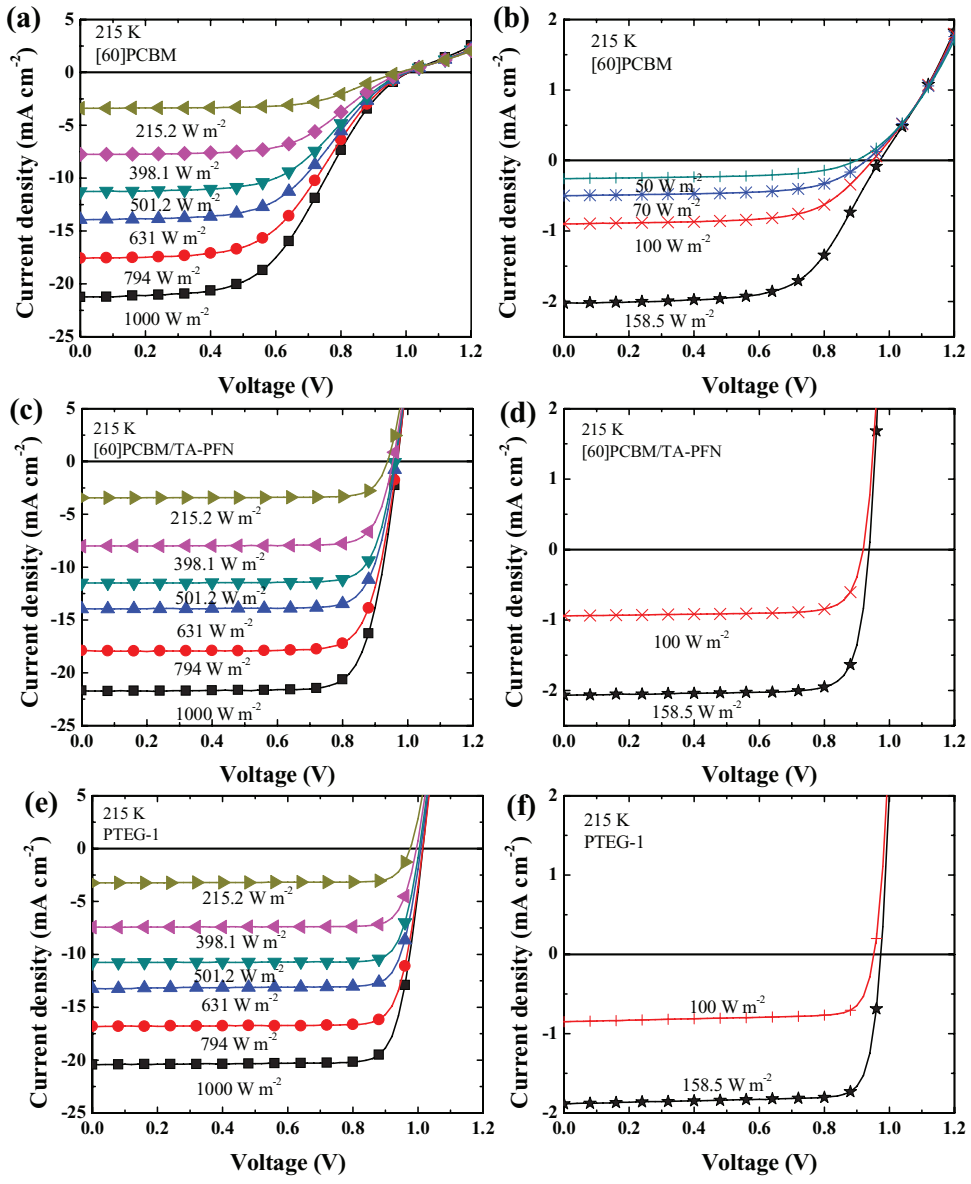

Figure 8. *J–V* curves measured at 215 K under different light intensities for device using a,b) [60]PCBM as EEL, c,d) [60]PCBM/TA-PFN as EEL, and e,f) PTEG-1 as EEL.

pronounced S-shape in the *J–V* curves with the reduction of the illumination intensity possibly due to the better balance between photogeneration and extraction of charge carriers. On the contrary, devices using n-doped [60]PCBM or PTEG-1 EELs do not show variations in the *J–V* characteristics shape with the light intensity variation.

3. Conclusion

In conclusion, we investigated how the perovskite film morphology and the EELs affect the temperature dependence of the device performance in p–i–n planar HPSCs. We found that the electron transport capability of the EEL dominates the temperature dependence of the charge extraction. The poor electron transport capability of [60]PCBM leads to a build-up of the electron concentration and a strong interfacial recombination in HP devices at low temperature. When PTEG-1 (or n-doped [60]PCBM layers) is used as EEL, the electrons are extracted to the cathode efficiently independently of the temperature due to its high electron transport capability, which results in HPSCs of high efficiency over a broad temperature range.

4. Experimental Section

Materials: CH_3NH_3I was purchased from Luminescence Technology Corporation. PEDOT:PSS water dispersion (Clevios VP AI 4083) was acquired from Heraeus. $PbCl_2$ (99.99%), Dimethylformamide (DMF) (99.8%), and chloroform (99.8%) were acquired from Sigma-Aldrich.

[60]PCBM (99.5%) was acquired from Solenne BV. PTEG-1 was synthesized according to the published method.[16]

Device Fabrication: Devices were fabricated following the same recipe reported in one of our previous works.[17] Briefly, ITO coated glass substrates were sonicated sequentially in detergent, deionized water, aceton, and isopropanol for 20 min each step. After drying at 140 °C for 10 min, the ITO substrates were subjected to the UV ozone cleaning treatment for 20 min. Then a 45 nm thick PEDOT:PSS layer was spin coated onto the ITO substrates and dried at 140 °C for 10 min. A 300 nm thick $CH_3NH_3PbI_{3-x}Cl_x$ layer was obtained by spin coating a precursor solution (40% wt) composed of CH_3NH_3I and $PbCl_2$ with a 3:1 molar ratio on top of PEDOT:PSS at 3000 rpm for 30 s, which was stored in high vacuum ($<10^{-6}$ mbar) for 12 h. The thermal annealing was performed on the aforementioned substrates at 100 °C for 1 h in a nitrogen-filled glove box. Then, a 50 nm thick $PC_{60}BM$ or PTEG-1 layer (10 mg mL^{-1} in chloroform) was deposited on top of the perovskite layer. N-type doping of [60]PCBM by PFN was realized by spin-coating 0.4 mg mL^{-1} PFN in CH_3OH:CH_3COOH (500:1 volume ratio) at 3000 rpm for 30 s, thermal annealing was performed at 100 °C for 10 min. N-type doping of [60]PCBM by LiF was realized by thermal evaporation of a 1 nm thick LiF layer on top of the fullerene derivative film, the structure was then thermally annealed at 100 °C for 10 min. The device structure was completed by evaporating 100 nm thick Al in high vacuum $<1 \times 10^{-6}$ mbar.

Characterization of the Perovskite Solar Cells: The current density–voltage characteristics of the perovskite solar cells were measured by a Keithley 2400 source meter under simulated AM 1.5 G solar illumination using a Steuernagel Solar constant 1200 metal halide lamp in a nitrogen filled glove box. The light intensity was calibrated to be 100 mW cm^{-2} by using an Si reference cell and correcting the spectral mismatch. A shadow mask (0.04 cm^2) was used to exclude the lateral contributions beyond the device area.

Steady State and Time-Resolved PL Measurement: The second harmonic (400 nm) of a Ti:sapphire laser (Coherent, Mira 900, repetition rate 76 MHz) was used to excite the samples. The optical emission was spectrally dispersed with a spectrometer and recorded by a cooled ImagEM Charge Coupled Device (CCD) camera from Hamamatsu. Time resolved PL spectra were detected using a Hamamatsu streak camera working in single-sweep mode. The excitation density was reduced to 1.4 µJ cm^{-2} by a neutral density filter, and the samples were mounted in a cryostat in nitrogen-filled glove box without exposure to air. All the PL measurements were conducted in the vacuum.

Morphology Characterization: Scanning Electron Microscope (SEM) topographical images were recorded on an XL 30 Envrionmental Scanning Electron Microscope (ESEM).

Conductivity Measurement: For the electrical conductivity measurements, parallel line-shape Au electrodes with width (w) of 13 mm and channel length (L) from 100 to 300 µm were deposited as top contacts. Voltage-sourced two-point conductivity measurements were performed in a probe station in an N_2-filled glove-box. Temperature dependent conductivity was measured under vacuum in a cryogenic probe station. The electrical conductivity (σ) was calculated according to the formula: $\sigma = (J/V) \times L/(w \times d)$. The conductivity of the commercial PEDOT:PSS (Clevios P VP AI 4083) was measured to be 0.06 S m^{-1}, which is consistent with the standard value between 0.02 and 0.2 S m^{-1}.

Supporting Information

Supporting Information is available from the Wiley Online Library or from the author.

Acknowledgements

The authors would like to thank the financial support from European Commission, Marie Curie Actions—Intra-European Fellowships (IEF) "SECQDSC" No. 626852 and European Research Council, ERC Starting Grant "HySPOD" No. 306983. The authors highly appreciate D. M. Balazs for the discussion about the charge transport in fullerenes and the effort to revise the paper. The authors also appreciate the technical support of A. Kamp. This is a publication by the Fundamenteel Onderzoek der Materie (FOM) Focus Group "Next Generation Organic Photovoltaics," participating in the Dutch Institute for Fundamental Energy Research (DIFFER).

Conflict of Interest

The authors declare no conflict of interest.

Keywords

charge extraction, electron transport layer, n-type doping, perovskite solar cells, temperature dependent

Received: May 14, 2017
Revised: June 15, 2017
Published online: September 7, 2017

[1] A. Kojima, K. Teshima, Y. Shirai, T. Miyasaka, *J. Am. Chem. Soc.* **2009**, *131*, 6050.
[2] H.-S. Kim, C.-R. Lee, J.-H. Im, K.-B. Lee, T. Moehl, A. Marchioro, S.-J. Moon, R. Humphry-Baker, J.-H. Yum, J. E. Moser, M. Grätzel, N.-G. Park, *Sci. Rep.* **2012**, *2*, 591.
[3] J. Burschka, N. Pellet, S.-J. Moon, R. Humphry-Baker, P. Gao, M. K. Nazeeruddin, M. Grätzel, *Nature* **2013**, *499*, 316.
[4] M. M. Lee, J. Teuscher, T. Miyasaka, T. N. Murakami, H. J. Snaith, *Science* **2012**, *338*, 643.
[5] J. Liu, S. Lu, L. Zhu, X. Li, W. C. H. Choy, *Nanoscale* **2016**, *8*, 3638.
[6] A. Mei, X. Li, L. Liu, Z. Ku, T. Liu, Y. Rong, M. Xu, M. Hu, J. Chen, Y. Yang, M. Grätzel, H. Han, *Science* **2014**, *345*, 295.
[7] S. Shao, Z. Chen, H.-H. Fang, G. H. ten Brink, D. Bartesaghi, S. Adjokatse, L. J. A. Koster, B. J. Kooi, A. Facchetti, M. A. Loi, *J. Mater. Chem. A* **2016**, *4*, 2419.
[8] F. Wang, H. Yu, H. Xu, N. Zhao, *Adv. Funct. Mater.* **2015**, *25*, 1120.
[9] B. Conings, J. Drijkoningen, N. Gauquelin, A. Babayigit, J. D'Haen, L. D'Olieslaeger, A. Ethirajan, J. Verbeeck, J. Manca, E. Mosconi, F. De Angelis, H.-G. Boyen, *Adv. Energy Mater.* **2015**, *5*, 1500477.
[10] R. K. Misra, S. Aharon, B. Li, D. Mogilyansky, I. Visoly-Fisher, L. Etgar, E. A. Katz, *J. Phys. Chem. Lett.* **2015**, *6*, 326.
[11] M. Saliba, T. Matsui, J.-Y. Seo, K. Domanski, J.-P. Correa-Baena, M. K. Nazeeruddin, S. M. Zakeeruddin, W. Tress, A. Abate, A. Hagfeldt, M. Grätzel, *Energy Environ. Sci.* **2016**, *9*, 1989.
[12] R. E. Beal, D. J. Slotcavage, T. Leijtens, A. R. Bowring, R. A. Belisle, W. H. Nguyen, G. F. Burkhard, E. T. Hoke, M. D. McGehee, *J. Phys. Chem. Lett.* **2016**, *7*, 746.
[13] D. Bryant, S. Wheeler, B. C. O'Regan, T. Watson, P. R. F. Barnes, D. Worsley, J. Durrant, *J. Phys. Chem. Lett.* **2015**, *6*, 3190.
[14] L. Cojocaru, S. Uchida, Y. Sanehira, V. Gonzalez-Pedro, J. Bisquert, J. Nakazaki, T. Kubo, H. Segawa, *Chem. Lett.* **2015**, *44*, 1557.
[15] H. Zhang, X. Qiao, Y. Shen, T. Moehl, S. M. Zakeeruddin, M. G. Atzel, M. Wang, *J. Mater. Chem. A* **2015**, *3*, 11762.
[16] F. Jahani, S. Torabi, R. C. Chiechi, L. J. A. Koster, J. C. Hummelen, *Chem. Commun.* **2014**, *50*, 10645.
[17] S. Shao, M. Abdu-Aguye, T. S. Sherkar, H.-H. Fang, S. Adjokatse, G. ten Brink, B. J. Kooi, L. J. A. Koster, M. A. Loi, *Adv. Funct. Mater.* **2016**, *26*, 8094.

[18] S. Shao, M. Abdu-Aguye, L. Qiu, L.-H. Lai, J. Liu, S. Adjokatse, F. Jahani, M. E. Kamminga, G. H. ten Brink, T. T. M. Palstra, B. J. Kooi, J. C. Hummelen, M. A. Loi, *Energy Environ. Sci.* **2016**, *9*, 2444.
[19] M. J. Speirs, D. N. Dirin, M. Abdu-Aguye, D. M. Balazs, M. V. Kovalenko, M. A. Loi, M. A. Loi, *Energy Environ. Sci.* **2016**, *9*, 2916.
[20] E. Ahlswede, J. Hanisch, M. Powalla, *Appl. Phys. Lett.* **2007**, *90*, 163504.
[21] C. J. Brabec, S. E. Shaheen, C. Winder, N. S. Sariciftci, P. Denk, *Appl. Phys. Lett.* **2002**, *80*, 1288.
[22] H. Wu, F. Huang, Y. Mo, W. Yang, D. Wang, J. Peng, Y. Cao, *Adv. Mater.* **2004**, *16*, 1826.
[23] Y. Shao, Z. Xiao, C. Bi, Y. Yuan, J. Huang, *Nat. Commun.* **2014**, *5*, 5784.
[24] K. Wojciechowski, S. D. Stranks, A. Abate, G. Sadoughi, A. Sadhanala, N. Kopidakis, G. Rumbles, C.-Z. Li, R. H. Friend, A. K.-Y. Jen, H. J. Snaith, *ACS Nano* **2014**, *8*, 12701.
[25] E. M. Hutter, J.-J. Hofman, M. L. Petrus, M. Moes, R. D. Abellon, P. Docampo, T. J. Savenije, *Adv. Energy Mater.* **2017**, *7*, 1602349.
[26] R. L. Milot, G. E. Eperon, H. J. Snaith, M. B. Johnston, L. M. Herz, *Adv. Funct. Mater.* **2015**, *25*, 6218.
[27] S. D. Stranks, V. M. Burlakov, T. Leijtens, J. M. Ball, A. Goriely, H. J. Snaith, *Phys. Rev. Appl.* **2014**, *2*, 34007.
[28] D. E. Markov, C. Tanase, P. W. M. Blom, J. Wildeman, *Phys. Rev. B* **2005**, *72*, 45217.
[29] N. I. Craciun, J. Wildeman, P. W. M. Blom, *Phys. Rev. Lett.* **2008**, *100*, 56601.
[30] T. Menke, D. Ray, J. Meiss, K. Leo, M. Riede, *Appl. Phys. Lett.* **2012**, *100*, 093304.
[31] S. Torabi, J. Liu, P. Gordiichuk, A. Herrmann, L. Qiu, F. Jahani, J. C. Hummelen, L. J. A. Koster, *ACS Appl. Mater. Interfaces* **2016**, *8*, 22623.